Crystal Structures of *Escherichia coli* Glycerol Kinase Variant S58→W in Complex with Nonhydrolyzable ATP Analogues Reveal a Putative Active Conformation of the Enzyme as a Result of Domain Motion[†,‡]

Cory E. Bystrom,[§,||] Donald W. Pettigrew,[⊥] Bruce P. Branchaud,[§] Patrick O'Brien,[§] and S. James Remington*[,§]

Institute of Molecular Biology, Departments of Physics and Chemistry, University of Oregon, Eugene, Oregon 97403, and Department of Biochemistry and Biophysics, Texas A&M University, College Station, Texas 77483

Received October 15, 1998; Revised Manuscript Received January 15, 1999

ABSTRACT: *Escherichia coli* glycerol kinase (GK) displays "half-of-the-sites" reactivity toward ATP and allosteric regulation by fructose 1,6-bisphosphate (FBP), which has been shown to promote dimer−tetramer assembly and to inhibit only tetramers. To probe the role of tetramer assembly, a mutation (Ser58→Trp) was designed to sterically block formation of the dimer−dimer interface near the FBP binding site [Ormo, M., Bystrom, C., and Remington, S. J. (1998) *Biochemistry 37*, 16565−16572]. The substitution did not substantially change the Michaelis constants or alter allosteric regulation of GK by a second effector, the phosphocarrier protein IIA^{Glc}; however, it eliminated FBP inhibition. Crystal structures of GK in complex with different nontransferable ATP analogues and glycerol revealed an asymmetric dimer with one subunit adopting an open conformation and the other adopting the closed conformation found in previously determined structures. The conformational difference is produced by a ∼6.0° rigid-body rotation of the N-terminal domain with respect to the C-terminal domain, similar to that observed for hexokinase and actin, members of the same ATPase superfamily. Two of the ATP analogues bound in nonproductive conformations in both subunits. However, β,γ-difluoromethyleneadenosine 5′-triphosphate (AMP-PCF_2P), a potent inhibitor of GK, bound nonproductively in the closed subunit and in a putative productive conformation in the open subunit, with the γ-phosphate placed for in-line transfer to glycerol. This asymmetry is consistent with "half-of-the-sites" reactivity and suggests that the inhibition of GK by FBP is due to restriction of domain motion.

Glycerol kinase (GK,[1] EC 2.7.1.30) catalyzes the transfer of the γ-phosphoryl of ATP to glycerol in the rate-limiting step of glycerol metabolism in *E. coli*. Stringent regulation of catalysis by GK is necessary to prevent the accumulation of toxic levels of biochemical intermediates and nonpreferential use of glycerol in the presence of glucose (*1*, *2*). Given this central role, it is unsurprising that GK shows complex regulatory behavior. Allosteric regulation by two effectors has been described (*3*−*8*). In these reports, the phosphoenolpyruvate phosphotransferase system (PTS) protein IIA^{Glc} (M_r 18 000, III^{Glc} in older literature) and a product of glycolysis, fructose 1,6-bisphosphate (FBP), were characterized as noncompetitive inhibitors of GK. FBP has been shown to alter the dimer−tetramer equilibrium, inactivating the tetramers (*3*−*5*). In addition, apparent negative cooperativity with respect to ATP concentration and "half-of-the-sites" reactivity have been observed toward ATP; that is, there is one low-affinity and one high-affinity ATP binding site per enzyme dimer (*7*, *8*), suggestive of some inherent asymmetry in the subunits.

The action of the allosteric effectors is to change V_{max} rather than K_m which categorizes the enzyme as a velocity-modulated system (*9*). Recent work demonstrated that IIA^{Glc} was an uncompetitive inhibitor with respect to both substrates (*10*), but this does not change the *V* system nature of the enzyme. *V* system allosteric regulation is rare, and the structural basis for such control has not been elucidated. However, clues regarding the mechanism for allosteric control of GK have been found by considering closely related proteins.

GK is a member of the sugar kinase/heat shock cognate 70/actin superfamily of ATPases which share a common, repeated $\beta\beta\beta\alpha\beta\alpha\beta\alpha$ fold (*11*). Catalysis by these enzymes is known to be accompanied by a large conformational change which is associated with interdomain motion (*11*). This motion has been characterized for hexokinase and actin via a number of biophysical techniques, including X-ray crystallography (*12*−*18*). Experimental evidence for con-

[†] This research was supported by NIH Grants GM-42618 (S.J.R.) and GM-49992 (D.W.P.) and by NSF Grant MCB-9311514 (B.P.B.).

[‡] Coordinates for the three nucleotide analogue/GK complex structures presented here are deposited with the Brookhaven Protein Data Bank under accession codes 1GLJ, 1GLL, and 1BWF.

* Corresponding author. E-mail: jim@uoxray.uoregon.edu.

[§] University of Oregon.

[||] Current address: Pharmacia and Upjohn, 7255-209-102, 301 Henrietta St., Kalamazoo, MI 49009.

[⊥] Texas A&M University.

[1] Abbreviations: GK, recombinant glycerol kinase from *E. coli*; PTS, phosphotransferase system; FBP, fructose 1,6-bisphosphate; NEM, *N*-ethylmaleimide; DTNB, 5,5′-dithiobis(1-nitrobenzoic acid); ATP, adenosine 5′-triphosphate; AMP-PCAs, γ-arsono-β,γ-methyleneadeonsine 5′-diphosphate; AMP-PCF_2P, β,γ-difluoromethyleneadenosine 5′-triphosphate; AMP-PCP, β,γ-methyleneadenosine 5′-triphosphate; ds-DNA, double-stranded DNA.

10.1021/bi982460z CCC: $18.00
Published on Web 03/04/1999

formational changes in GK has been obtained by indirect methods. Glycerol and a range of adenine nucleotides protect GK from inactivation by DTNB or NEM (*19*), and ATP protects GK from proteolytic cleavage (*20*). It has been hypothesized that the action of FBP and IIA^{Glc} is to perturb the energetics of domain motion which is associated with catalysis. Enzymes with amino acid substitutions that perturb domain−domain interactions affect inhibition by both allosteric effectors (*20*, *21*). However, these results do not provide insight into the nature of the conformational transitions associated with catalysis or its regulation.

The X-ray crystallographic structure of GK/IIA^{Glc} in complex with glycerol and ADP was determined at 2.6 Å resolution by Hurley et al. (*22*). The structure revealed a tetrameric arrangement of monomers (tetramer I) in the unit cell with each monomer binding a single factor IIA^{Glc} molecule. A dimer−dimer assembly interface was proposed to be formed by the interaction of two pairs of antiparallel helices with one helix (GK residues 49−68) donated from each monomer. Further investigation of this interface indicated its biological relevance through the observation that the amino acid substitutions A65→T and D72→N altered the dimer−tetramer equilibrium and made GK insensitive to FBP inhibition (*23*). Recently, the structure of GK in a new space group was determined (*24*) which allowed the FBP binding site to be identified by X-ray crystallography. Mutation of an FBP ligand (Arg 236) to Ala eliminated inhibition (*24*) and confirmed that the structure was indeed a physiologically relevant, inactive tetramer (tetramer II) as originally proposed by de Riel and Paulus (*4*, *5*). Tetramer I, which is different from tetramer II due to a rotation and translation of one dimer relative to the other, is most likely an artifact of crystallization as tetramer II has now been observed in three different crystal forms (*24*, *25*). However, the dimer−dimer interface in both tetramers is comprised of the same sets of helices.

Despite the insight gained from these studies, the structural basis for the inhibition of GK by either of the allosteric effectors has not been forthcoming. The available crystallographic structures of GK, in the presence and absence of either allosteric effector, have not shown significant domain motion or structural rearrangement within the monomers, which led to the proposal that all of the structures are representative of inhibited forms of the enzyme. This is exemplified in previous work with the GK variant A65→T (*25*). Although the substitution was known to disrupt dimer−tetramer equilibrium in solution (*23*), the crystal structure of this variant (*25*) is essentially identical to the symmetric tetramer found in the FBP-bound form of the enzyme (*24*). This result suggested that crystal growth conditions/packing interactions could overcome some amount of unfavorable steric interactions at the dimer−dimer regulatory interface. Finally, all of the tetrameric forms have *222* symmetry, giving no clue as to why the enzyme displays "half-of -the-sites" reactivity toward ATP, which presumably must result in an asymmetry inherent to the active form of the molecule. Therefore, our strategy was to construct and crystallize a mutant GK molecule that is unable to form tetramers, in the hopes of obtaining a presumptive active conformation.

In the present study, site-directed mutagenesis was utilized to aggressively disrupt the regulatory dimer−dimer interface of GK associated with FBP inhibition by insertion of a tryptophan (S58→W) into the tightly associated, relatively polar dimer−dimer interface. Three nontransferable ATP analogues, shown in Figure 1, were utilized during crystallization to investigate potential active site changes which resulted from disruption of the regulatory interface. The X-ray crystal structures of the GK/nucleotide analogue complexes revealed an asymmetric dimer of GK monomers where one of the monomers displayed a ~6.0° rigid-body rotation between the major domains which form the active site cleft, opening up the cleft. The analogues AMP-PCAs and AMP-PCP appear to bind in nonproductive modes in both the open and closed subunits while AMP-PCF_2P binds in a nonproductive orientation in the closed subunit and a putative productive conformation in the open chain. Based on the observed domain motion and binding of AMP-PCF_2P, it is proposed that this structure represents the first view of an active form of GK and offers the opportunity to present a more complete structural model for the inhibition of GK by FBP.

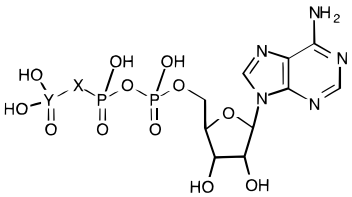

1) AMP-PCF_2P: X = CF_2, Y = P
2) AMP-PCAs: X = CH_2, Y = As
3) AMP-PCP: X = CH_2, Y = P

FIGURE 1: Nonhydrolyzable ATP analogues utilized in this study.

MATERIALS AND METHODS

Materials. Restriction endonucleases and Vent polymerase for PCR were purchased from New England Biolabs. The Muta-Gene In Vitro Mutagenesis Kit was purchased from Bio-Rad Laboratories. DNA purification kits were purchased from Qiagen. The PET-28b expression system was purchased from Novagen. Oligonucleotides were purchased from Gibco, and DNA sequencing was performed on an Applied Biosystems 377 automated sequencer at the Biotechnology Laboratories at the University of Oregon. The nontransferable nucleotide triphosphate analogues (AMP-PCAs, AMP-PCF_2P) were prepared as part of this study, and the synthesis and characterization have been reported elsewhere (*26*). AMP-PCP and other reagents were purchased from Sigma.

Mutagenesis and Cloning. Site-directed mutagenesis was accomplished with the Muta-Gene In Vitro Mutagenesis Kit utilizing a M13mp19 construct containing the glpK gene (*23*) and a mutagenic oligo with the sequence 5′CCAGCGTccaGCTTTGG3′. Complete nucleotide sequencing confirmed the presence of the desired mutation and the integrity of the glpK gene. The ssDNA containing the S58W mutation and the glpK gene was amplified via PCR utilizing primers which contained restriction endonuclease sites for *Nco*I at the 5′-end (5′GAATCCATGGGCGAAAAAAAATATATCGTTGCGCTC3′) and *Xho*I at the 3′-end (ATCTTACTCGAGTTACATTATTCGTCGTGTTCTTCCC) of the final construct. The amplification products were digested and ligated into *Nco*I/*Xho*I digested PET-28b. The resulting plasmid was used to transform *E. coli* XL1-Blue cells. Complete nucleotide sequencing of the dsDNA from several transformants

confirmed the presence of the mutation and the integrity of the entire gene with the exception of the expected conversion of Thr at position 2 to Gly as a result of utilizing the *Nco*I restriction site for cloning. This plasmid was then introduced into BL21(DE3) cells for expression.

Purification. Purification of the mutant glycerol kinase was carried out as previously described with minor modifications (*27*). Purified protein was concentrated to ~5 mg/mL and flash-frozen in liquid nitrogen and stored at −80 °C until needed.

Enzyme Activity and Kinetic Studies. Enzyme assays were measured using the previously described, ADP-coupled, spectrophotometric assay (*7*). Initial velocity studies were carried out as described previously.

Gel-Permeation Chromatography. One milliliter aliquots of 0.5 mg/mL GK samples in 0.1 M triethanolamine hydrochloride buffer at pH 7.0, 2 mM glycerol, with or without 2 mM FBP, were applied to a Sephadex G-200 column connected to a Pharmacia FPLC system. A flow rate of 0.3 mL/min at a pressure less than 0.3 MPa at was maintained, and the effluent was monitored by UV absorption at 280 nm. The column was calibrated by using the following molecular weight standards: apoferritin (480 000), γ-globulin (160 000), bovine serum albumin (67 000), and ovalbumin (48 000). Retention volumes were taken as the volume at which each standard eluted from the column with highest absorbance. A calibration curve was determined by plotting the logarithm of the molecular weight of each standard versus retention volume. Experimental molecular weights for wild type and variant glycerol kinase were determined from the calibration curve.

Crystallization and Data Collection. Crystals of glycerol kinase variant S58W in complex with each of the three nontransferable ATP analogues and glycerol were obtained via the hanging-drop vapor diffusion method and improved by seeding. Prior to crystallization, the enzyme was concentrated to 12 mg/mL as described (*24*). Hanging drops were prepared by mixing 5 μL of protein with 5 μL of precipitant (20% PEG 1000, 0.3 M $MgCl_2$, and 0.1 M Pipes, pH 6.5), 1 μL of 1 M NaCl, and 1 μL of 100 mM inhibitor and equilibrated over wells containing 1 mL of precipitant. Small, disordered crystals appeared within 3 days. These small crystals were harvested for seeding by washing repeatedly in precipitant solution containing 10% PEG 1000. Fresh drops were prepared as described above with the exception that the PEG concentration was reduced to 16%. A single seed was placed in each drop, and crystals suitable for data collection grew within 48 h. The crystals were exceptionally fragile and required careful mounting in flattened capillaries to avoid loss of diffraction. Precession photography indicated that this crystal form belonged to space group $C222_1$. A V_m value of 2.6 Å^3/Da was calculated based on the presence of a dimer in the asymmetric unit (*28*).

Diffraction data were collected on a San Diego Multiwire Detector Mark III area detector mounted on a Rigaku RU-100 rotating anode generator fitted with a graphite monochromator and operated at 40 kV, 150 mA. Three crystals were used to collect a complete data set for each complex which was reduced using the software supplied with the detector (*29*).

Molecular Replacement and Refinement. The structure of GK S58W in complex with AMP-PCAs was solved by standard molecular replacement techniques followed by refinement with TNT (*30*). A glycerol kinase monomer without waters or ligands from the $P2_1$ crystal form (PDB accession code 1GLF) was used as a search model. The *B*-factors for all atoms of the search model were set to the Wilson B of the data set as calculated in the CCP4 package (*31*). The rotation search was carried out using the direct rotation function in X-PLOR (*32*) utilizing data from 10 to 3.5 Å. The highest peak, and correct rotation solution for placement of one of the monomers, was 10 σ above the mean. The next highest peak was 5 σ above the mean. Using this solution from the rotation search, a translation search was performed with AMORE (*33*). A single translation solution was found with a peak height of 8 σ. A second monomer was not successfully located by this strategy. Five cycles of rigid body refinement were carried out on the properly placed monomer, and $2F_o - F_c$ electron density maps were calculated at 4.0 Å resolution. Upon examination of the electron density maps with the graphics package O (*34*), the location of the second monomer in the asymmetric unit became evident. The second monomer was placed manually although the density for the N-terminal 300 amino acids was weak. The initial *R*-factor for the starting model was 44.9% for data from 20 to 3.5 Å.

Model improvement began with rigid-body refinement in three rounds utilizing the entire dimer, followed by individual monomers. Data from 6 to 4 Å were utilized. The final round of rigid-body refinement was carried out with each monomer divided into two domains: an N-terminal domain consisting of residues 2−245 and a C-terminal domain consisting of residues 246−499. The first four rounds of model building and positional refinement were carried out utilizing non-crystallographic symmetry constraints between the N-terminal and C-terminal domains while allowing regions of the protein involved in crystal contacts and the hinge region of the protein to refine without constraints. Data from 20 to 3.5 Å were utilized. At this point, the $F_o - F_c$ maps revealed strong positive density for a glycerol molecule and a nucleotide analogue at the active site of the enzymes which were modeled in. In the final round of refinement, the resolution limits were extended to 3.0 Å, a magnesium atom was modeled into the active site (identified by earlier manganese soaking studies; Feese, M. D., personal communication), and tightly restrained correlated *B*-factor refinement was carried out. Due to the limited resolution of the data, no solvent was modeled in.

The structures of the complexes of glycerol kinase with AMP-PCP and AMP-PCF_2P were solved using the coordinates of the AMP-PCAs structure after removal of the ligands.

Structural Analysis. Analyses of hinge bending angles were performed with the Hingefind algorithm (*35*) and EDPDB (*36*). Gap volumes and surface areas were calculated using the program SURFNET (*37*). Three-dimensional superpositions of the catalytic cores of glycerol kinase, hexokinase, and actin were calculated with the program Superimpose (*38*). A Quicktime movie of the domain motion calculated by an experimental web server is available at http://bioinfo.mbb.yale.edu/MolMovDB.

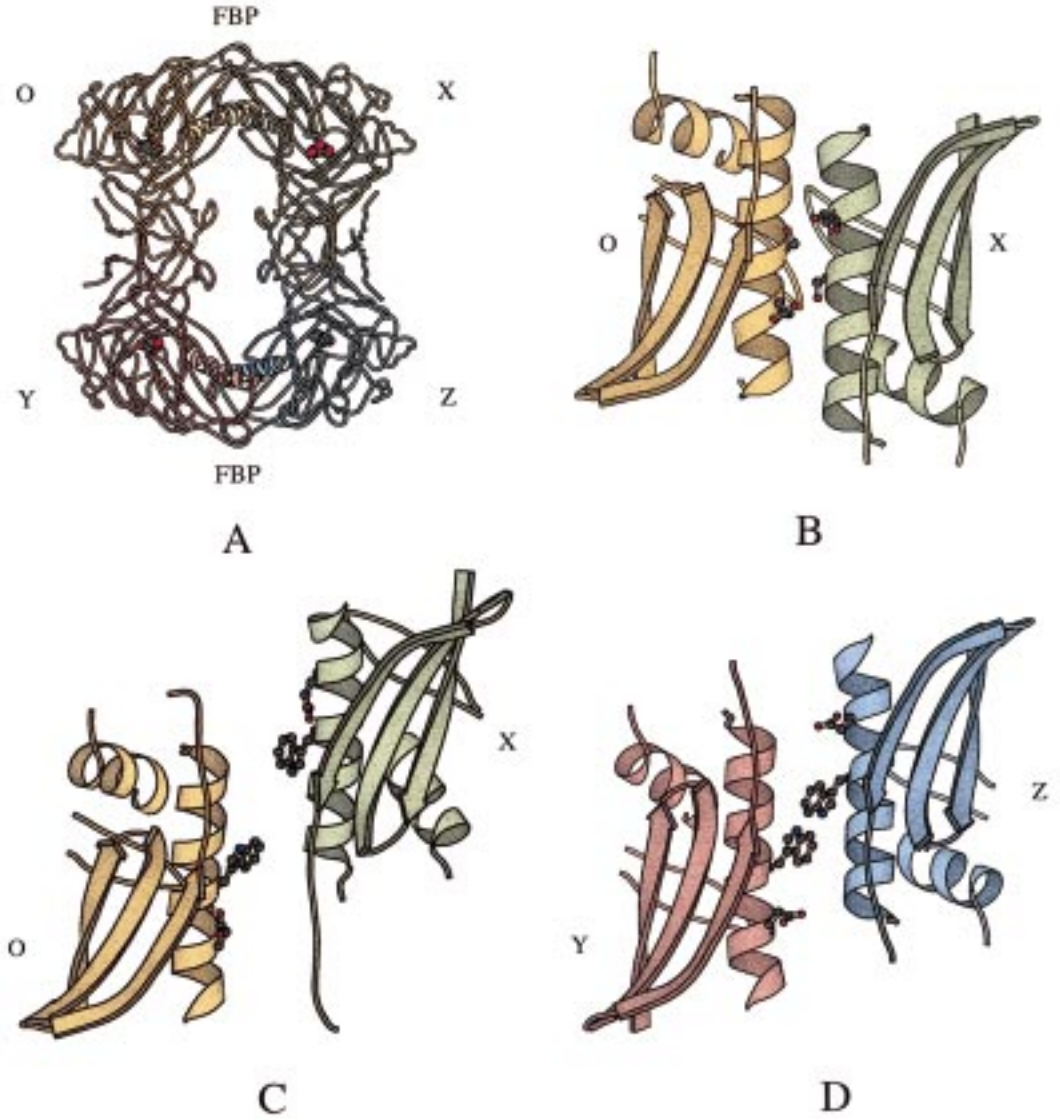

FIGURE 2: (A) MOLSCRIPT (*58*) schematic drawing of the wild-type GK tetramer showing subunit nomenclature. The FBP binding and the regulatory interfaces are at the top and bottom of the illustration, with FBP binding centrally located at the O/X and Y/Z interface. FBP binds between the two loops at the very top and bottom of the illustration. The loops at the center of the tetramer do not contact each other and are not part of the dimer−dimer interface. Glycerol is shown in a space-filling representation revealing the central location of the active site. (B) The physiologically relevant regulatory O/X or Y/Z interface of GK (tetramer II). Serine 58 and Glu 62 from each monomer are represented as balls and sticks. (C) The O/X crystal contact of the $C222_1$ crystal form of the S58W variant showing the 14 Å shift in register of the two antiparallel helices at the interface. (D) The O/X crystal contact of the $C222_1$ crystal form showing the 7 Å shift in register of the two helices.

RESULTS AND DISCUSSION

Design and Characterization of the Variant. A difficulty in interpreting the structural consequences of allosteric effector binding has been the apparent lack of a structure of a putative active form of GK. A significant barrier to solving this problem is the fact that high protein concentrations required for crystal growth experiments drive tetramer formation and lead to crystallization of inactive forms of the enzyme (*25*). However, inspection of the dimer−dimer interface suggested that additional mutagenesis would be advantageous if the interface could be more severely disrupted. The regulatory interface is formed by contact of two antiparallel helices (residues 49−68 from each monomer) between the O and X chains of GK in the FBP complex (Figure 2 A,B). At this crystal contact, Ser 58 from one monomer makes a hydrogen bond across the tetramer interface to Glu 62 of the other monomer. The antiparallel packing of the helices at this interface and tetrameric arrangement of GK duplicate this interaction 4 times within each tetramer. Elimination of this interaction could be achieved by any of a number of substitutions. However, it seemed clear that the greatest degree of disruption would be achieved by substitution of a tryptophan for Ser 58 which would eliminate the hydrogen bonds as well as adding steric bulk.

The biochemical consequences of this substitution were expected to be elimination of FBP inhibition while leaving IIA^{Glc} regulation and catalysis unchanged. Inhibition experiments (Figure 3) and gel permeation experiments (Table 2) confirmed that the S58W substitution abolishes inhibition of GK by FBP via disruption of the dimer−tetramer assembly reaction. Inhibition by IIA^{Glc} was unchanged compared to wild type. The kinetic constants derived from initial velocity studies gave V_{max} 79 units/mg, K_{ATP} 23 μM, $K_{glycerol}$ 14 μM,

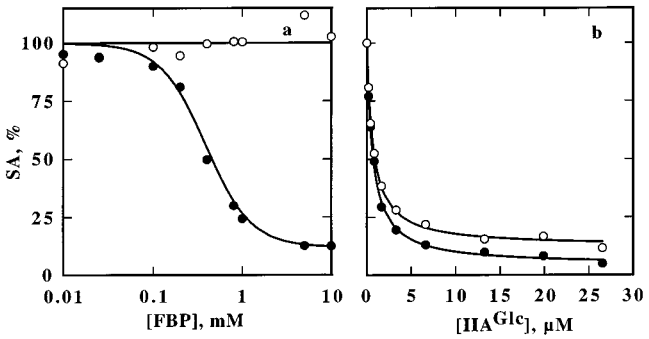

FIGURE 3: Inhibition of wild-type (●) and variant S58W (○) glycerol kinase by (a) FBP and (b) IIA^{Glc}. The specific activities of the glycerol kinases were determined at pH 7.0, 25 °C, 0.3 μg/mL, 2.0 mM glycerol, and 2.5 mM ATP, with the indicated concentrations of FBP or IIA^{Glc} determined using the coupled assay described under Materials and Methods. For IIA^{Glc} inhibition studies, 0.1 mM $ZnCl_2$ was added. Results are shown as a percentage of relative specific activity measured in the absence of inhibitor.

Table 1: Data Collection and Refinement Statistics

	inhibitor complex		
	AMP-PCAs	AMP-PCP	AMP-PCF_{2P}
no. of crystals	3	3	3
resolution (Å)	3.0	3.0	3.0
total obsd	64416	53041	84144
unique obsd	25966	20445	24796
completeness (%)	90	83	95
R_{merge} (%)	7.5	6.8	7.1
cell parameters			
a (Å)	99.67	99.77	99.76
b (Å)	200.70	201.15	200.29
c (Å)	114.73	114.34	114.74
β (deg)	90	90	90
refinement statistics			
resolution range (Å)	20−3.0	20−3.0	20−3.0
no. of protein atoms	7820	7820	7813
R-value[b] (%)	16.8	17.6	16.8
rms deviations from ideals[a]			
lengths (Å)	0.020	0.019	0.018
angles (deg)	2.929	2.826	2.945
B correl ($Å^2$)	3.37	3.59	3.79
Ramachandran analysis			
no. residues favorable + additionally allowed	861	863	855
no. generously allowed	12	8	6
no. disallowed	1	3	3
NCS agreement (rms Å)			
N-terminal domain	0.31	0.33	0.33
C-terminal domain	0.34	0.34	0.36

[a] Target values are 0.02 Å for bond lengths and planarity, 3.0° for bond angles, and 6.0 $Å^2$ for restrained *B* factors of high-resolution (∼1.6 Å) structures. [b] $R_{crystallographic} = \Sigma||F_{obs}| - |F_{calc}||/\Sigma|F_{obs}|$.

and $K_{i,ATP}$ 108 μM. The activity of this variant is significantly higher than wild-type GK, and the Michaelis constants are increased slightly compared to wild type [V_{max} 15.3 units/mg, K_{ATP} 8.4 μM, $K_{glycerol}$ 4.9 μM, and $K_{i,ATP}$ 86 μM (*21*)]. The kinetic data indicate that the substitution does not substantially alter the active site of the enzyme.

Structure of GK Mutant S58W. The GK variant S58W, in complexes with three different nontransferable ATP analogues, crystallized in space group $C222_1$, and data could be collected to 3.0 Å resolution. The crystals contain a dimer in the asymmetric unit that corresponds to the functional O/Y dimer according to the established notation (*11*). The crystallographic *R*-factors for the refined models are 16.8, 17.6, and 16.8% for the AMP-PCAs, AMP-PCP, and AMP-PCF_2P complexes, respectively. Rms deviations between parts of the model related by noncrystallographic symmetry were less than 0.40 Å. The models have satisfactory geometry, and detailed statistics are reported in Table 1. A Ramachandran analysis indicated the models to be of adequate quality given the moderate resolution with no less than 97.3% of the residues in the most favored and additionally allowed regions of phi/psi space and no more than 3 residues in disallowed regions. Residues in disallowed regions were in regions of poor electron density, so that a more stereochemically reasonable interpretation of their conformations could not be made.

Table 2: Effect of FBP on the Apparent Molecular Weight of Glycerol Kinases[a]

	apparent molecular weight	
enzyme	no FBP	2 mM FBP
S58W	109 000	109 000
wild type	109 000	182 000

[a] Apparent molecular weights were estimated by size-exclusion chromatography on Sephadex G200 as described under Materials and Methods.

Most interesting was the observation that the dimer in the asymmetric unit of the crystal is asymmetric with one monomer in a closed conformation and the second monomer adopting a open conformation which had not been previously observed. Despite the substitution, the dimers nevertheless form crystal contacts in a manner which resembles the dimer−dimer interfaces of tetramer II in the FBP-bound form (Figure 2A,B). The asymmetry of the monomers results in crystal packing interactions at the former O/X and Y/Z interfaces which responded differently to accommodate the S58W substitution. The helices at the O/X contact undergo a shift leading to a 14 Å increase in the distance between the Cα atoms of residue 58 from the O and X chains (Figure 2C) when compared to the same distance measured in the FBP-bound tetramer (Figure 2B) which was used to design the substitution. The Y/Z contact undergoes a smaller, but still substantial 7 Å increase in distance between Cα atoms of residue 58 from each monomer at the interface (Figure 2D). The loops forming the FBP binding site (residues 231−236) are mostly disordered and are not visible in the electron density maps for either monomer.

The asymmetric crystal packing interactions did not have a substantial impact on the O/Y interface of the functional dimer, which is formed by interactions between the C-terminal domains of each monomer. In addition, an examination of crystal packing interactions, other than the ones at the regulatory tetramer interface, did not suggest that any other contacts played a direct role in changing the conformation.

The superposition of the Cα coordinates of the Y chain of variant S58W with a monomer from any of the previously determined GK structures resulted in an overall rms deviation of about 0.4 Å compared to a ∼0.9 Å rms deviation for similar Cα superpositions of the O chain. This suggested that the Y chain was essentially identical to previously determined GK structures while the O chain was substantially

FIGURE 4: Representation of the hinge axis between the O and Y chains of the S58W variant in the presence of AMP-PCF$_2$P. Hinge axis calculated with the Hingefind algorithm. Hinge statistics: 6.2° rotation, 10.2% relative error. Image displayed with MIDAS and rendered with Conic (*59*, *60*).

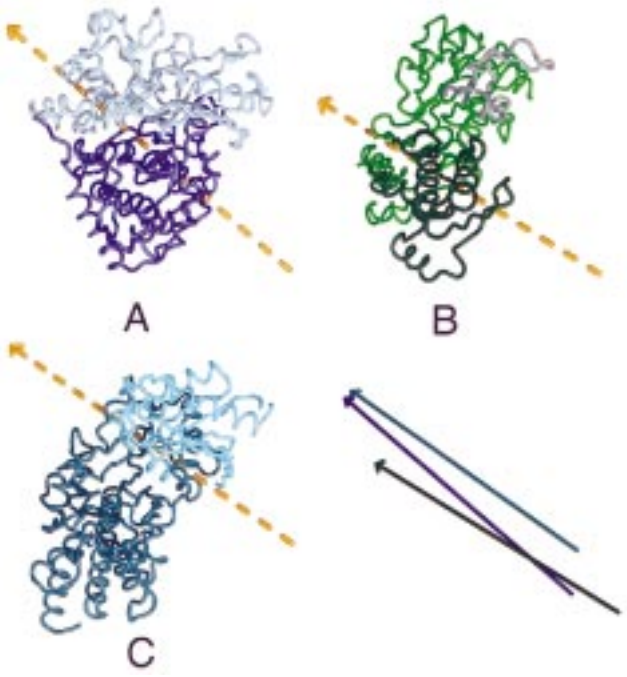

FIGURE 5: Representation of the hinge axes superimposed on the closed forms of (A) glycerol kinase, (B) actin, and (C) hexokinase. Hinge axes were calculated with the slow partitioning function of the Hingefind algorithm implemented in XPLOR. Independent domains identified by the Hingefind algorithm are highlighted by light/dark shading. Statistics for each hinge calculation are: glycerol kinase, 6.2° rotation, relative error 10.2%; actin, 8.6° rotation, relative error 6.87%; hexokinase, 10.9° rotation, 1.33% relative error. Image displayed in MIDAS and rendered with Conic (*59*, *60*). After superposition of the catalytic cores of the three enzymes, the superpositions of the hinge axes are shown at lower right.

different. Utilization of the Hingefind algorithm (*35*) to analyze domain motion between the O and Y chains identified an effective rotation angle of ~6.0° between domains I and II in all three variant GK/nucleotide analogue complex structures (Figure 5). Calculation of the hinge bending angle with EDPDB (*36*) gave similar results utilizing domain I and domain II. To ensure that the NCS constraints used during refinement did not unduly influence the location and magnitude of the hinge, a test refinement without NCS constraints was carried out. The location and magnitude of the hinge bending angle were not substantially affected.

Successful refinement of the structure utilizing tight domain-wise NCS constraints and the results from the Hingefind algorithm (Figure 4) indicate that the individual N- and C-terminal domains are very similar between the O and Y chains. While the C-terminal domains, related by noncrystallographic symmetry, superimpose with an rms of not more than 0.45 Å, the N-terminal domains (after C-terminal domain superposition) have rms deviations of >1.6 Å. This suggests that domain repositioning is a result of rigid-body movement rather than rearrangement of secondary structure elements. Cα−Cα difference distance plots confirm this, showing very few features within the individual domains but very large features between domains (data not shown). An analysis of the structural details of hinge binding is limited by the low resolution of the data which precludes a meaningful analysis of phi/psi torsion angles to residues explicitly involved in hinge bending (*39*, *40*). While it is possible that secondary structure element rearrangements are an important part of the domain motion of GK, the mechanism of domain repositioning in these structures is unlikely to utilize a small number of large torsion angle rearrangements. The complexity and tight packing of the regions of the protein between the two domains which make up the active site cleft appear to require a suite of smaller structural changes to achieve the observed domain motion as proposed by Gerstein (*41*). This domain motion is another crystallographic example of domain motion observed for proteins in this superfamily, and, thus, GK joins hexokinase (*12*, *13*, *42*) and actin (*14*, *18*) which have also been demonstrated to undergo conformational change. In addition, the effects of substitutions in or near the domain−domain interface on the catalytic and regulatory properties of GK are consistent with this conformational change (*20*, *21*).

Comparison of Domain Motion in GK, Hexokinase, and Actin. A wealth of biochemical and structural information available for hexokinase and actin has demonstrated the relationship between domain motion and catalysis for this superfamily of proteins. Comparison of the motion of GK to hexokinase and actin reveals several important features. The domain motion in GK is observed in the presence of glycerol and nucleotide analogues for both the open and closed chains. In contrast, the open conformation of one form of hexokinase contains *O*-toluolylglucosamine at the active site (*43*, *44*) while the closed conformation contains bound glucose (*12*, *13*). Neither hexokinase structure contains nucleotide at the active site although model complexes have been built (*42*). Additionally, the domain motion in GK is smaller in magnitude than in hexokinase; GK domain superposition is achieved by a ~6.0° rotation and 0.2 Å

translation along a unique axis compared to a 12° rotation and 0.3 Å translation for hexokinase (*13*, *35*).

Analysis of the hexokinase structures by Bennett focused on the characterization of an induced-fit mechanism when glucose bound to the protein (*12*). In addition to the crystallographic evidence, a number of kinetic and biophysical studies linked the conformational change associated with glucose binding to solvent exclusion necessary for efficient catalysis (*45*). The similarity between GK and hexokinase suggests that GK in solution should also have a very open ligand-free structure which closes substantially upon binding of glycerol. This is supported by experiments which have shown that, in the presence of glycerol, GK is protected from heat and chemical (DTNB, NEM) inactivation (*8*, *19*). However, because the crystallographically determined domain motion of GK variant S58W is observed in the presence of both glycerol and nucleotide analogue, it is unlikely that the motion is associated with the formation of the initial enzyme/substrate complex as described for hexokinase. Supporting this assumption, glycerol is deeply buried in both the open and closed monomers and is not substantially accessible to solvent. Also, solvent accessibility of the triphosphate chain of the analogue increases only slightly in the open monomer. This evidence suggests that the observed domain motion may be associated with a catalytic step or allosteric transition rather than substrate binding event. Therefore, this structure is unlikely to represent a very open form of the enzyme which would be sensitive to heat and chemical inactivation. A structure of GK in the absence of substrates could help confirm this, but suitable crystals have not yet been obtained.

Lesk and Gerstein have analyzed the motion of hexokinase and concluded that domain motion is accompanied by secondary structural element rearrangement composed of the movement of helices with respect to helices and β-sheets (*41*, *46*). In contrast, the GK hinge bending observed in this study does not appear to require secondary structure element rearrangement.

An open form of profilin/β-actin was reported which resulted from changing the ionic strength of the buffer in which crystals were equilibrated (*14*). This structure revealed a suite of conformational changes which was more elaborate than the domain motion observed in a comparison of the DNase I/α-actin complex with a profilin/β-actin complex (*47*). This structure also revealed a change in nucleotide binding as a result of domain motion which was coined "bond ratcheting". The repositioning of the ATP, which was coupled to the associated cleft opening, increased the solvent-accessible surface of the ATP phosphates by 50 Å^2. However, this motion did not appear to involve a transition from a nonproductive to productive binding mode of the nucleotide. The hinge motion between the major domains of actin was measured to be ~9.6°. The motion is in agreement with computational studies (*14*, *17*) and is comparable in magnitude to GK.

Despite the differences in magnitude of domain motion, state of ligand binding, and overall 3-dimensional architectures of the proteins compared, the direction of motion and relative location of the hinge between the domains which form the active site clefts are strikingly similar (Figure 5). After three-dimensional superposition of the catalytic cores of GK, actin, and hexokinase in the open and closed conformations, the corresponding hinge axes are nearly parallel and lie very close to one another in three-dimensional space. This similarity is in agreement with the proposal that architecturally related proteins will undergo similar domain motion (*41*).

Binding of Ligands at the Active Site. The active site of GK is located in a cleft that is situated between domains I and II. Clearly, the observation of hinge bending motion between these domains suggested concomitant changes at the active site. The structures of the GK variant S58W were obtained in complex with one of three interesting nontransferable ATP analogues, either AMP-PCF$_2$P, AMP-PCAs, or AMP-PCP (Figure 1). Additionally, each structure contains modeled glycerol and a magnesium ion (based on manganese soaks) in similar conformation to previously determined structures. The adenosine moiety of each ATP analogue bound in a similar configuration to that which was observed previously (*22*, *25*). However, substantial differences in the orientation of the triphosphate analogue chain were apparent.

The binding of the triphosphate chain in the AMP-PCF$_2$P complex was especially striking. The open (O) monomer bound the fluoromethylene analogue in what appears to be an active conformation (Figure 6, top) while the closed (Y) monomer bound in a nonproductive conformation (Figure 6, bottom). In the open monomer, the difluoromethylene triphosphate moiety is oriented to position the γ-phosphate to within 4.7 Å of the O3 of glycerol, reasonably positioned for an in-line transfer, expected for GK on the basis of the chiral phosphate studies (*48*) which demonstrated an inversion of stereochemical configuration of the γ-phosphoryl group of ATP upon transfer to glycerol by GK. In contrast, the closed monomer bound the fluoromethylene analogue in a clearly nonproductive conformation which placed the γ-phosphonate in contact with the β-turn formed by residues 12−15, positioned over 7 Å from the nucleophilic O3 position of glycerol. While the binding of the fluorinated ATP analogue is suggestive of an active conformation, comparison of the binding of AMP-PCF$_2$P in the open chain with ATP bound to the active site of actin and Hsc70 reinforces this conclusion. The conformation of AMP-PCF$_2$P is in good agreement with the binding of ATP in both actin and Hsc70, which may represent active forms of enzyme [Figure 7 (*14*, *49*)]. It is particularly interesting to note that the asymmetry of the dimer and the binding of the difluoromethyl-ATP analogue are consistent with the known half-of-the-sites reactivity and negative cooperativity with respect to ATP concentration (*7*, *8*), which implies that an active form of GK is inherently asymmetric.

The methylene bisphosphonate (AMP-PCP) and arsonomethylene phosphonate AMP-PCAs) chains assume a conformation which places the γ-phosphonate or γ-arsonate in contact with the β-turn formed by residues 12−15 in both the open and closed monomers. This orientation is very similar to the conformation of AMP-PCF$_2$P in the closed momoner. For AMP-PCAs (Figure 8), the nonproductive conformation in the closed monomer is stabilized by hydrogen bonds between the oxyanion of the γ-arsonate and both the backbone amide protons of the β-turn and the Oγ of Thr 14 (3.2 Å).

In each monomer, Arg 17 makes contact with Asp 437 rather than the phosphoryl oxygens of the ATP analogues. In the GK/IIA^{Glc} complex, Arg 17 was observed to change

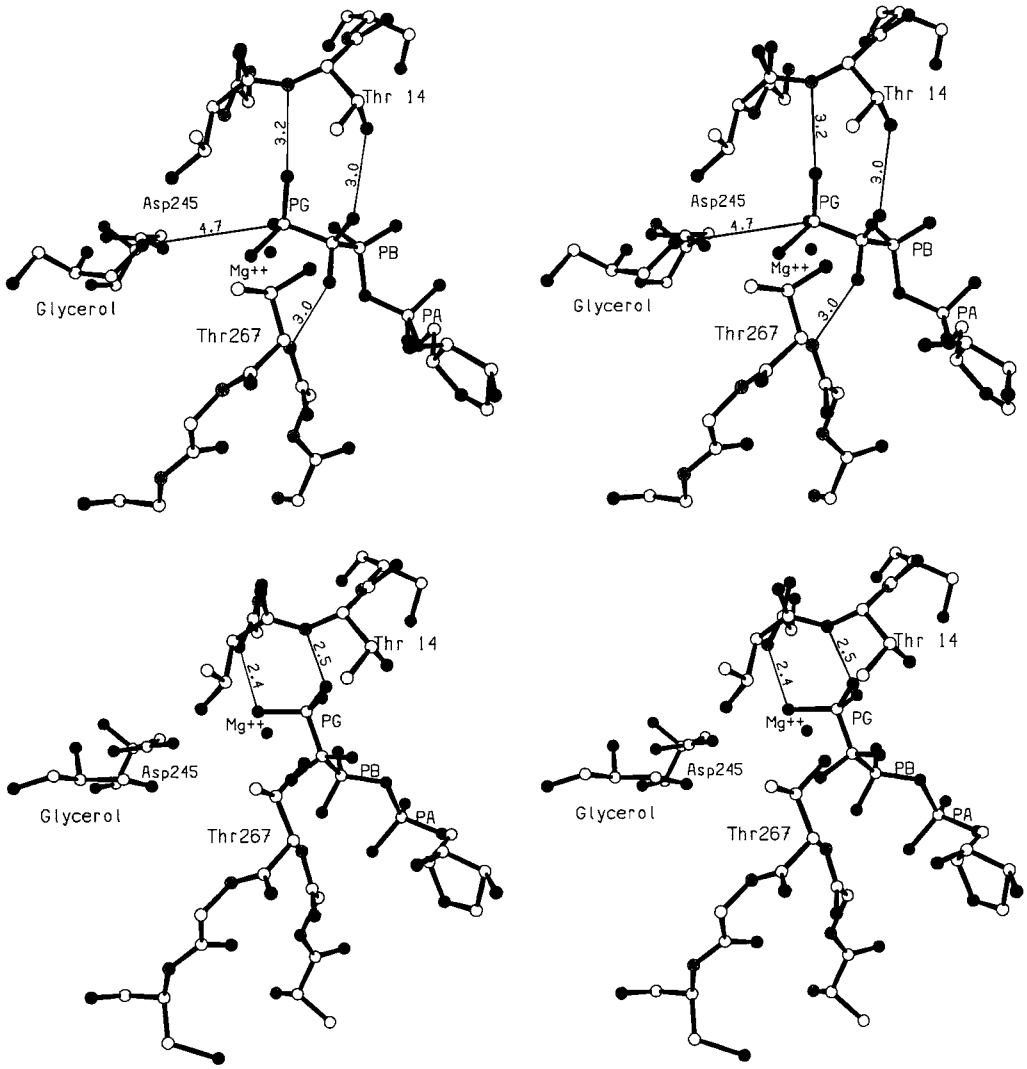

FIGURE 6: ORTEP representation of the binding of AMP-PCF_2P in the (top) open and (bottom) closed chains of GK variant S58W.

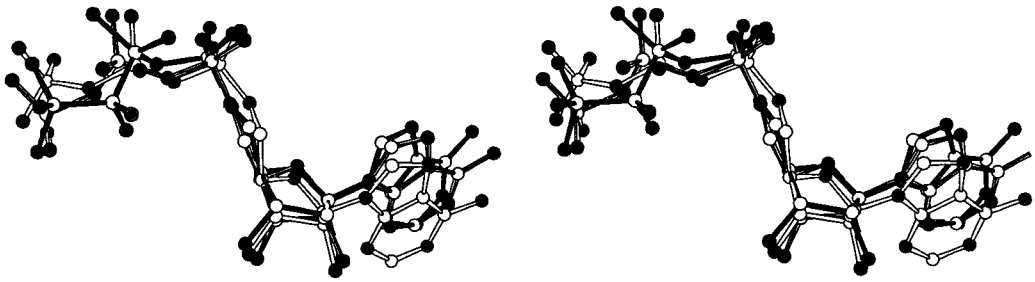

FIGURE 7: Superposition of AMP-PCF_2P from the open chain of GK and ATP from Hsc70 and the profilin/β-actin complex. Three-dimensional superpositions were achieved through overlays of the ribose ring. AMP-PCF_2P from GK is drawn in dark bonds; ATP from actin in open bonds; ATP from profilin/β-actin in shaded bonds.

orientation when ADP was present at the active site (*22*) and interact with two of the phosphoryl oxygens at the β-position of ADP. The reason for this difference is unclear but may be related to the fact that the S58W structures contain substrate analogues rather than product.

It has long been known that the ability of different nontransferable ATP analogues to inhibit ATPases depends on the particular enzyme (*50*). Previously, we compared inhibition of GK by a range of ATP analogues (*26*), and K_i values indicated that AMP-PCF_2P was a superior inhibitor. Blackburn and Thatcher have suggested that the superiority of fluoromethyl phosphonates is related to the fact they are isosteric, isopolar, and have similar torsion angle energetics when compared to their parent phosphates (*51*, *52*). Our results indicate that AMP-PCF_2P behaves differently than other ATP analogues in the context of the GK active site. This study, along with an earlier report of the crystal structure of adenylate kinase with AMP-PCF_2P (*53*), suggests that this analogue may be quite valuable in revealing features of nucleotide binding and mechanistic details that may not be observed with alternative nontransferable analogues.

It appears that the ability of the fluorines to participate in favorable hydrogen bonding interactions which are precluded in the methylene-substituted analogues may be especially

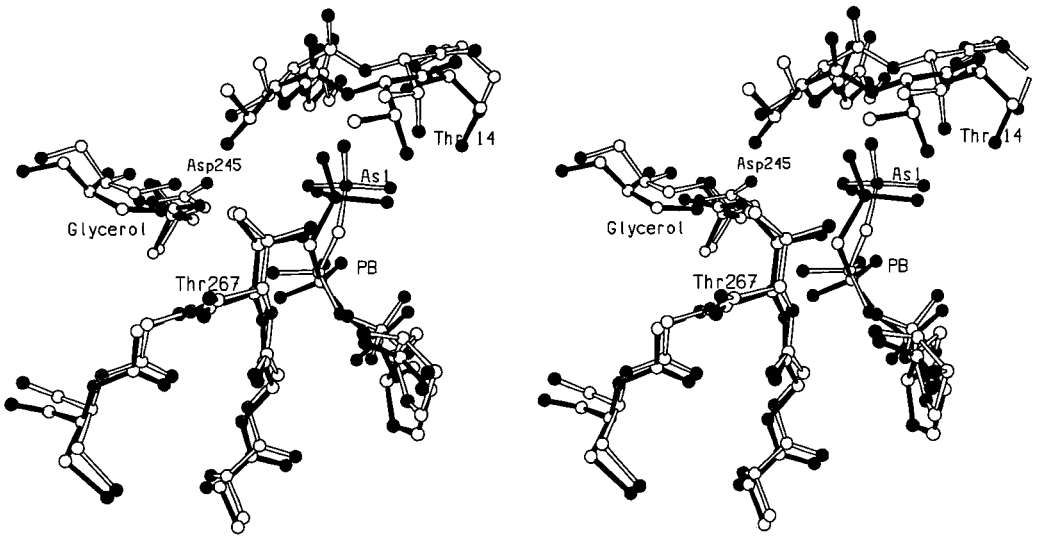

FIGURE 8: ORTEP representation of the binding of AMP-PCAs in the open and closed chains of GK variant S58W. The open conformation is shown in open bonds and the closed conformation in dark bonds. Binding of AMP-PCP in the open and closed conformations is nearly identical to that of AMP-PCAs.

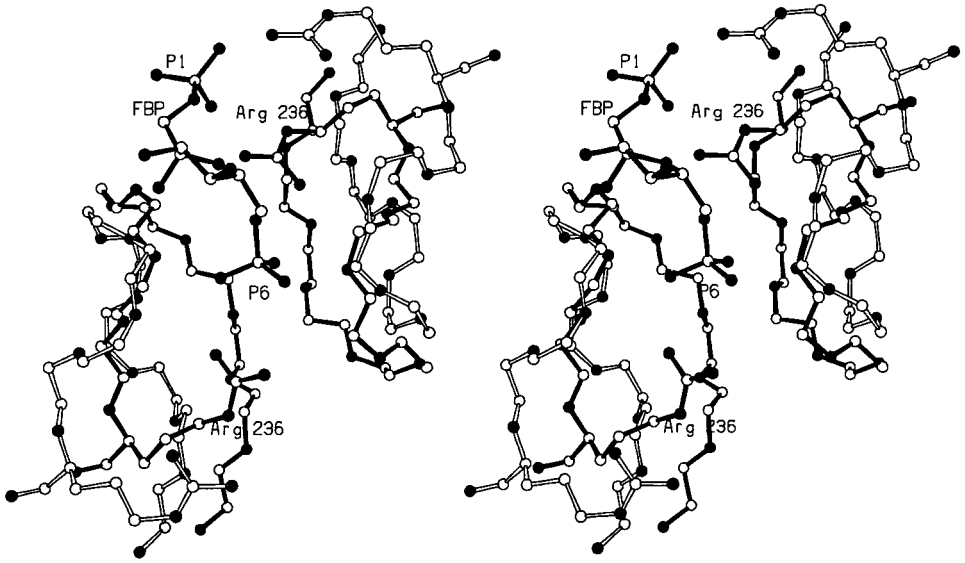

FIGURE 9: ORTEP view of the FBP binding site at the O/X interface of tetramer II (dark bonds) and the same site after application of the hinge motion observed in the crystal structure of the GK S58W variant (open bonds).

important. In the open monomer, fluorine F1 forms a close contact with the Oγ of Thr 14 (3.0 Å), and fluorine F2 interacts with the backbone amide hydrogen of Thr 267 (3.0 Å). In the closed monomer, fluorine F1 interacts with the Oγ of Thr 267 (3.2 Å), and fluorine F2 interacts with the backbone amide nitrogen of Thr 267 (3.0 Å). Opening of the domains increases the distance between the two $\beta1-\beta2$ loops which may reduce the ability for the γ-phosphate to interact with the β-turn associated with the N-terminal domain in the closed form of the enzyme. Subsequently, this may have allowed for the formation of alternate favorable interactions with the fluorines which lead to the dramatic repositioning of the fluorinated phosphonate chain. The inability of both the methylene arsonate and methylene phosphonate ATP analogues to form favorable interactions at the β,γ-bridging position to offset the loss of the hydrogen bonds at the γ-phosphate or γ-arsonate position may explain why they form nonproductive complexes in both the open and closed forms of GK. One possible interpretation is that the fluorines act as mimics of the oxygen lone pairs which would be present at the β,γ-bridging oxygen of ATP allowing AMP-PCF_2P to accurately mimic the binding of ATP (*51*, *52*, *54*−*56*).

Conformational Change and Possible Mode of Inhibition of GK by FBP. Based on the biochemical characterization and asymmetry of the S58W GK dimer, an analysis of crystal packing interactions, asymmetric of binding of AMP-PCF_2P, and comparison to previously determined structures (actin, hexokinase, and Hsc 70), we propose that the dimer, which makes up the asymmetric unit of the $C222_1$ crystal form of this variant, is representative of an active form of glycerol kinase where one monomer (O chain) represents an open, active conformation and the other monomer (Y chain) represents a tightly closed, inactive conformation of GK.

With the assumption that this variant has provided a structural example of the domain motion that is an essential part of the catalytic and regulatory mechanism of GK, it is possible to propose a detailed structural model for the mechanism of allosteric regulation by FBP. Based on the crystal structures available, it is clear that the transition of

GK from a closed to open conformation precludes formation of the FBP regulatory interface. A model building study was conducted with the inactive FBP-bound tetramer in which the hinge-bending motion was applied to the N-terminal domain of the O and X chains (Figure 9). This motion substantially shifts the loops involved in formation of the FBP binding site, eliminating the possibility of FBP binding as observed previously. Arg 236 and Gly 234 from each monomer were shown to be key elements in the inhibition of GK by FBP (*24*). Opening of the active site increases the distance between these residues such that the interaction with FBP is precluded, and, as discussed, these residues are disordered in the present crystal form. Based on these observations, it appears that assembly of the FBP-bound, tetrameric form of GK leads to a significant increase of the energetic barrier for opening of the active site cleft. Consequently, if opening of the cleft is necessary for efficient catalysis, then the inhibitory action of FBP is clear.

Despite this insight, relatively little is known about the dynamics of protein domain motion and how such motions are coupled to catalysis or regulation (*57*). However, computational studies and structural analysis of actin have indicated that hinge motions similar to the one characterized for GK in this study are low-energy conformational changes that are readily accessible (*14*, *16*, *17*). It is plausible to consider that the domain motion of GK observed in these structures leads to changes in binding of the triphosphate moiety. If the structure presented here indeed represents a catalytically active form of GK, then the velocity-modulated regulation may arise from the coupling of small-magnitude domain motions with the correct positioning of the triphosphate chain of ATP. In such a mechanism, the assembly of the FBP bound tetramer would alter the frequency with which the γ-phosphate position of ATP was productively bound and appropriately positioned for catalysis after the binding of both substrates.

Alternatively, the nonproductive binding of AMP-PCF_2P in the tightly closed chain may be artifactual since catalysis cannot occur with the nontransferable analogue. Therefore, it is also reasonable to propose that during normal catalysis, ADP and/or glycerol 3-phosphate would be trapped in the closed active site cleft and that the rate of product dissociation would be retarded by active site closure. In such a model, assembly of the FBP-bound tetramers would favor active site closure, coupling V_{max} regulation to the rate of product release. Experiments are underway which utilize disulfide cross-links to form covalently bonded tetramers and dimers to distinguish between these two possibilities.

Summary. The most important features of the structures presented here are the observation of an asymmetric dimer which arises from domain I−domain II motion within one monomer and the observation of asymmetric binding of the nontransferable ATP analogue AMP-PCF_2P. The available biochemical and structural evidence implies that the asymmetric dimer is representative of an active form of the enzyme with glycerol and the ATP analogue bound in a conformation approriate for an in-line transfer of the γ-phosphoryl group with inversion of stereochemistry. The domain motion in GK provides an additional example of large-scale conformational change observed via X-ray crystallography for a member of the sugar kinase/Hsc 70/actin superfamily. Considering the asymmetry of domain motion, differences in nucleotide analogue binding, and comparisons with related proteins, we propose that the observed domain motion of GK is related to a catalytic or allosteric transition. It seems likely that the velocity-modulated regulation of GK by FBP is associated with the regulation of the domain motion observed in these complexes.

ACKNOWLEDGMENT

We thank Donna Barker and Karen Kallio for their expert technical assistance.

REFERENCES

1. Freedberg, W. B., Kistler, W. S., and Lin, E. C. (1971) *J. Bacteriol. 108*, 137−144.
2. Zwaig, N., Kistler, W. S., and Lin, E. C. (1970) *J. Bacteriol. 102*, 753−759.
3. de Riel, J. K., and Paulus, H. (1978) *Biochemistry 17*, 5146−5150.
4. de Riel, J. K., and Paulus, H. (1978) *Biochemistry 17*, 5141−5145.
5. de Riel, J. K., and Paulus, H. (1978) *Biochemistry 17*, 1534−5140.
6. Novotny, M. J., Fredrickson, W. L., Waygood, E. B., and Saier, M. H. (1985) *J. Bacteriol. 162*, 810−816.
7. Pettigrew, D. W., Yu, G., and Liu, Y. (1990) *Biochemistry 29*, 8620−8627.
8. Thorner, J. W., and Paulus, H. (1973) *J. Biol. Chem. 248*, 3922−3932.
9. Monod, J., Wyman, J., and Changeaux, J. P. (1965) *J. Mol. Biol. 12*, 88−118.
10. Pettigrew, D. W., Meadow, N. D., Roseman, S., and Remington, S. J. (1998) *Biochemistry 37*, 4875−4883.
11. Hurley, J. H. (1996) *Annu. Rev. Biophys. Biomol. Struct. 25*, 137−162.
12. Bennett, W. S., and Steitz, T. A. (1978) *Proc. Natl. Acad. Sci. U.S.A. 75*, 4848−4852.
13. Bennett, W. S., and Steitz, T. A. (1980) *J. Mol. Biol. 140*, 211−230.
14. Chick, J. K., Lindberg, U., and Schutt, C. E. (1996) *J. Mol. Biol. 263*, 607−623.
15. Harrison, W. (1984) *Biopolymers 23*, 2943−2949.
16. Tirion, M., and ben-Avraham, D. (1993) *J. Mol. Biol. 230*, 186−195.
17. Wriggers, W., and Schulten, K. (1997) *Biophys. J. 73*, 624−639.
18. Miki, M. (1991) *Biochemistry 30*, 10878−10884.
19. Pettigrew, D. W. (1986) *Biochemistry 25*, 4711−4718.
20. Pettigrew, D. P., Liu, W., Holmes, C., Meadow, N., and Roseman, S. (1996) *J. Bacteriol. 178*, 2846−2852.
21. Pettigrew, D. W., Smith, G. B., Thomas, K. P., and Dodds, D. C. (1997) *Arch. Biochem. Biophys. 349*, 236−245.
22. Hurley, J. H., Faber, H. R., Worthylake, D., Meadow, N., Roseman, S., Pettigrew, D. W., and Remington, S. J. (1993) *Science 259*, 673−677.
23. Liu, W. Z., Faber, R., Feese, M., Remington, S. J., and Pettigrew, D. W. (1994) *Biochemistry 33*, 10120−10126.
24. Ormo, M., Bystrom, C. E., Pettigrew, D. W., and Remington, S. J. (1998) *Biochemistry 37*, 16565−16572.
25. Feese, M. D., Faber, R. H., Bystrom, C. E., Pettigrew, D. W., and Remington, S. J. (1998) *Structure 6*, 1407−1418.
26. Bystrom, C. E., Pettigrew, D., and Remington, S. J. (1997) *Bioorg. Med. Chem. Lett. 7*, 2613−2616.
27. Faber, R., Pettigrew, D. W., and Remington, S. J. (1989) *J. Mol. Biol. 207*, 637−639.
28. Matthews, B. W. (1968) *J. Mol. Biol. 33*, 491−497.
29. Howard, A. J., Nielsen, C., and Xuong, N. H. (1985) *Methods Enzymol. 114*, 542−471.
30. Tronrud, D. E. (1992) *Acta Crystallogr. A48*, 912−916.
31. CCP4 (1994) *Acta Cyrstallogr. D50*, 760−763.
32. Brunger, A. T. (1992) Yale University Press, New Haven, CT.
33. Navaza, J. (1994) *Acta Crystallogr. A50*, 238−291.

34. Jones, T. A., Zou, J. Y., Cowan, S. J., and Kjeldgaard, M. (1991) *Acta Crystallogr. A47*, 110−119.
35. Wriggers, W., and Schulten, K. (1997) *Proteins: Struct., Funct., Genet. 29*, 1−14.
36. Zhang, C. X.-J., and Matthews, B. W. (1995) *J. Appl. Crystallogr. 28*, 624−630.
37. Lakowski, R. A. (1995) *J. Mol. Graph. 13*, 323−330.
38. Diederichs, K. (1995) *Proteins: Struct., Funct., Genet. 23*, 187−195.
39. Page, R., Lindberg, U., and Schutt, C. E. (1998) *J. Mol. Biol. 280*, 463−474.
40. Korn, A. P., and Rose, D. R. (1994) *Protein Eng. 7*, 961−967.
41. Gerstein, M., Lesk, A. M., and Chothia, C. (1994) *Biochemistry 33*, 6739− 6749.
42. Steitz, T. A., Shosham, M., and Bennett, W. S. (1981) *Philos. Trans. R. Soc. London B 293*, 43−52.
43. Anderson, C. M., Stenkamp, R. E., McDonald, R. C., and Steitz, T. A. (1978) *J. Mol. Biol. 123*, 15−33.
44. Anderson, C. M., Stenkamp, R. E., McDonald, R. C., and Steitz, T. A. (1978) *J. Mol. Biol. 123*, 207−219.
45. McDonald, R. C., Steitz, T. A., and Engelman, D. M. (1979) *Biochemistry 18*, 338−342.
46. Lesk, A. M., and Chothia, C. (1984) *J. Mol. Biol. 174*, 175−191.
47. Schutt, C. E., Lindberg, U., Myslik, J., and Strauss, N. (1993) *Nature 365*, 810−816.
48. Blattner, W. A., and Knowles, J. (1979) *Biochemistry 18*, 3927−3933.
49. Flaherty, K. M., Wilbanks, S. M., DeLuca-Flaherty, C., and McKay, D. B. (1994) *J. Biol. Chem. 269*, 12899−12907.
50. Yount, R. G., Babcock, D., Ballantyne, W., and Ojala, D. (1971) *Biochemistry 10*, 2484−2489.
51. Blackburn, G. M. (1981) *Chem. Ind.* 134−138.
52. Thatcher, G. R., and Campbell, A. S. (1993) *J. Org. Chem. 58*, 2272−2281.
53. Schlauderer, G. J., Proba, K., and Schulz, G. E. (1996) *J. Mol. Biol. 256*, 223−227.
54. Blackburn, G. M., England, D. A., and Kolkmann, F. (1981) *J. Chem. Soc., Chem. Commun. 18*, 1188−1190.
55. Blackburn, G. M., England, D. A., and Kolkmann, F. (1981) *J. Chem. Soc., Chem. Commun. 17*, 930−932.
56. Blackburn, G. M., Kent, D. E., and Kolkmann, F. (1984) *J. Chem. Soc., Perkin Trans. 1*, 1118−1122.
57. Jardetzky, O. (1996) *Prog. Biophys. Mol. Biol. 65*, 171−219.
58. Kraulis, P. J. (1991) *J. Appl. Crystallogr. 24*, 946−950.
59. Ferrin, T. E., Huang, C. C., Jarvis, L. E., and Langridge, R. (1988) *J. Mol. Graphics 6*, 13−27.
60. Huang, C. C., Pettersen, E. F., Klein, T. E., Ferrin, T. E., and Langridge, R. (1991) *J. Mol. Graphics 9*, 230−236..

BI982460Z